Applied Physics Laboratory
University of Washington

1013 NE 40th Street
Box 355640
Seattle, WA 98105-6698

206-543-1300
FAX 206-543-6785
www.apl.washington.edu

30 September 2013

To: Dr. Robert H. Headrick
Office of Naval Research (ONR 322)
875 N. Randolph Street, Suite 1425
Arlington, VA 22203-1995

From: Steven G Kargl

Subj: ONR Grant: N00014-10-1-0114
"Generation of Synthetic SAS Data for Targets near the Seafloor: Propagation Component"

Encl: (1) Archival Journal Articles, Proceeding Papers and Oral Presentations, Abstracts for Oral Presentations
(2) *First International Conference and Exhibition on Underwater Acoustics, Corfu, Greece* Conference Proceedings: "Fast Acoustic Ray Model for the Scattering from Targets in Synthetic Aperture Sonar Applications"
(3) Benchmark model comparisons of the fast ray model deficiency and a wave propagation model
(4) SF298 for Enclosure

Enclosures (1-3) comprise the final report that closes the subject grant. Enclosure (4) is the SF298 form that will accompany the final report submission to DTIC.

Steven G Kargl

cc: Grant & Contract Administrator, APL-UW
Office of Sponsored Programs, UW
Naval Research Laboratory Code 5596
Defense Technical Information Center (electronic files with SF298)

Generation of Synthetic SAS Data for Targets near the Seafloor: Propagation Component

Steven G. Kargl
Applied Physics Laboratory, University of Washington,
1013 NE 40th St., Seattle WA 98105-6698
Phone: (206) 685-4677, FAX: (206) 543-6785, Email: kargl@apl.washington.edu

Award Number: N00014-10-1-0114
http://www.apl.washington.edu/projects/projects.php/

Overview:

This report contains three parts. First, a list of archival journal publications, conference proceedings, and abstracts for oral presentations are listed. It is noted that the research reported in these papers and presentations was performed in conjunction with "Generation of Synthetic SAS Data for Targets near the Seafloor: Propagation Component," (ONR Award N00014-07-G-0557/0023). Second, the fast ray model for target scattering in a homogeneous waveguide has yet to be published in an archival journal, but an overview has been given in the conference proceedings for the *First International Conference and Exhibition on Underwater Acoustics, Corfu, Greece*. As this proceedings paper is currently only available from the conference website and its availability may not be ensured, the paper is included in this final report. Finally, recent benchmark model comparisons of the fast ray model and a wave propagation model, based on the trapped modes in propagation in a homogeneous Pekeris waveguide, revealed an significant deficiency in the implementation of fast ray model. The details of the deficiency and the correction to the implementation of the fast ray model are given in a section that follows the proceedings paper.

Enclosure 1

Archival Journal Articles:

1 SG Kargl, KL Williams, and EI Thorsos, "Synthetic aperture sonar imaging of simple finite targets," *IEEE J. Ocean. Eng.*, **37**(3), 516-532 (2012).

2 M Zampolli, AL Espana, KL Williams, SG Kargl, EI Thorsos, JL Lopes, JL Kennedy, and PL Marston, "Low- to mid-frequency scattering from elastic objects on a sand seafloor: simulation of frequency and aspect dependent structural echoes," *J. Comp. Acoust.*, **20**(2), p 1240007 (14 pages), DOI: 10.1142/S0218396X12400073, (2012).

3 KL Williams, SG Kargl, EI Thorsos, DS Burnett, JL Lopes, M Zampolli, and PL Marston, "Acoustic scattering from a solid aluminum cylinder in contact with a sand sediment: Measurements, modeling, and interpretation," *J. Acoust. Soc. Am.*, **127**, 3356-3371, (2010).

Proceeding Papers and Oral Presentations:

1 SG Kargl, AL Espana, and KL Williams, "Fast acoustic ray model for the scattering from targets in synthetic aperture sonar applications," *1st Inter. Conf. Exhib. Underwater Acoust.*, 8 pages, ISBN: 978-618-80725-0-3, (2013), http://www.uaconferences.org/index.php/archive-past-uam-proceedings/ua2013-proceedings

2 SG Kargl, KL Williams, TM Marston, JL Kennedy, and JL Lopes, "Acoustic Response of Unexploded Ordnance (UXO) and Cylindrical Targets," *2010 OCEANS MTS/IEEE SEATTLE*, 5 pages, DOI: 10.1109/OCEANS.2010.5664392, (2010).

3 AL Espana, KL Williams, SG Kargl, M Zampolli, TM Marston, and PL Marston, "Measurements and modeling of the acoustic scattering from an aluminum pipe in the free field and in contact with a sand sediment," *2010 OCEANS MTS/IEEE SEATTLE*, 5 pages, DOI: 10.1109/OCEANS.2010.5664603, (2010).

Abstracts for Oral Presentations:

1 SG Kargl, KL Williams, AL Espana, "Fast model for target scattering in a homogeneous waveguide," *J. Acoust. Soc. Am.*, **132**, 1909 (2012).

2 KL Williams, AL Espana, SG Kargl, M Zampolli, "Submerged target scattering: comparison of combined finite element/simplified acoustics models to data," *J. Acoust. Soc. Am.*, **131**, 3393 (2012).

3 SG Kargl, KL Williams, AL Espana, JL Kennedy, TT M, JL Lopes, R Lim, "Acoustic scattering from underwater munitions near a water-sediment interface," *J. Acoust. Soc. Am.*, **129**, 2685 (2011).

4 AL Espana, KL Williams, SG Kargl, M Zampolli, "Acoustic scattering from proud and buried unexploded ordnances in a cluttered environment," *J. Acoust. Soc. Am.*, **129**, 2685 (2011)

5 AL Espana, KL Williams, SG Kargl, TM Marston, PL Marston, "Measured acoustic scattering from a water-filled aluminum pipe in contact with various interfaces," *J. Acoust. Soc. Am.*, **128**, 2461 (2010).

ENCLOSURE 2

FAST ACOUSTIC RAY MODEL FOR THE SCATTERING FROM TARGETS IN SYNTHETIC APERTURE SONAR APPLICATIONS

Steven G. Kargl[a], Aubrey L. España[a], Kevin L. Williams[a]

[a]Applied Physics Laboratory, University of Washington, 1013 NE 40th St., Box 355640, Seattle, WA 98105-6698.

Steven G. Kargl, Applied Physics Laboratory, University of Washington, 1013 NE 40th St., Box 355640, Seattle, WA 98105-6698; Fax: (206) 543-6785; Email: kargl@apl.washington.edu.

Abstract: *Monostatic synthetic aperture sonar (SAS) data sets for the scattering from a target in a waveguide can be simulated via a fast model that combines an acoustic ray approximation for propagation in the waveguide with far-field scattering from a target in free-space. With the assumption that acoustic rays arise from the source and receiver and their images, the problem of wave propagation and scattering from a target within the waveguide is replaced by a superposition of a set of free-field scattering problems. Under normal operating conditions, the separation distance between a SAS platform and a target is large compared to the carrier wavelength of the transmitted signal, and hence, the free-field scattered signal can be reduced to a far-field approximation where a spherically diverging wave is weighted by a scattering amplitude. The scattering amplitude contains all of the information about the scatterer (e.g., its material properties) and the directionality of the scattered field. A scattering amplitude can be obtained from a direct measurement or a finite-element analysis of a target. The fast ray model allows one, who is interested in SAS processing algorithms, to generate data sets with variations in the environment or source-receiver-target geometry without incurring the expense associated with the collection of actual SAS data. Results from the fast ray model will be compared to data and finite-element results for several targets in shallow water. The horizontal range to the targets and time gating permit the air-water interface to be ignored.*

Keywords: *Acoustic Ray Model, Synthetic Aperture Sonar, Scattering amplitude.*

1. INTRODUCTION

The use of synthetic aperture sonar (SAS) has become a standard modality for the detection of targets in marine environments [1-3]. In particular, SAS platforms that operate at frequencies below 50 kHz and with a wide bandwidth have several advantages over other sonar technologies (such as side-scan sonar, which can be limited in range and range resolution). Low-frequency, broad-bandwidth SAS platforms can provide longer detection ranges, the possibility of coupling into elastic modes of vibration of a target, and deeper penetration into sediments. Longer detection ranges are possible due to the lower attenuation of low-frequency sound in water. This then permits rapid wide-area surveys. In addition, the range resolution of a SAS platform is related to the bandwidth of the transmitted signal and is independent of the range to the target. Excitation of the elastic modes of vibration of a target offers a mechanism that may be exploited by classification algorithms to differentiate a target from clutter. With greater penetration depths into sediments, the detection of partially and completely buried targets becomes feasible. Kargl *et al* [2] recently presented a model to investigate the response of buried targets to a sonar signal. That model combined first-order perturbation theory for scattering from a rough surface and an approximation based on free-field scattering. This paper reports on a model that combines an acoustic ray model and free-field scattering for targets within the water column.

In the development and validation of automatic target recognition (ATR) algorithms, access to a large collection of SAS data sets for a given target in various environments and various targets in the same environment is desirable [4]. However, the *in-situ* collection of data in a marine environment can be time consuming, cost prohibitive, infeasible due to limited access to a particular environment, and subject to either changes to the environment during the collection period or a lack of measurement of environmental conditions. The model presented below allows one to fabricate SAS data for a target in a marine environment with the caveat that passive noise and reverberation must be obtained from an additional model (such as the model described in [2]). The generated SAS data sets can supplement other SAS data sets and aid in the development and validation of ATR algorithms.

2. ACOUSTIC RAY MODEL FOR TARGET SCATTERING

When the wavelength of sound is much smaller than the depth of a waveguide, the scattering of sound from a target within a homogeneous waveguide can be approximated by an acoustic ray model. The waveguide of interest here is a homogeneous layer of water between an upper semi-infinite half-space of air and a lower semi-infinite half-space of a homogenous sediment. Figure 1(a) depicts the scattering problem, and displays the direct path arrival as well as the ray paths that interact once with the upper and/or lower boundaries. By considering image sources and receivers reflected about the boundaries, one can associate acoustic ray paths with these images. Figure 1(b) depicts the image sources and receivers and their associated acoustic rays. Figure 1 also demonstrates the reduction of the waveguide scattering problem to an equivalent superposition of (possibly infinitely many) free-field scattering problems. In the model discussed here, the homogeneous sediment has been modeled as either an attenuating fluid with a frequency-independent loss parameter or as a fluid described by an effective density fluid model [5].

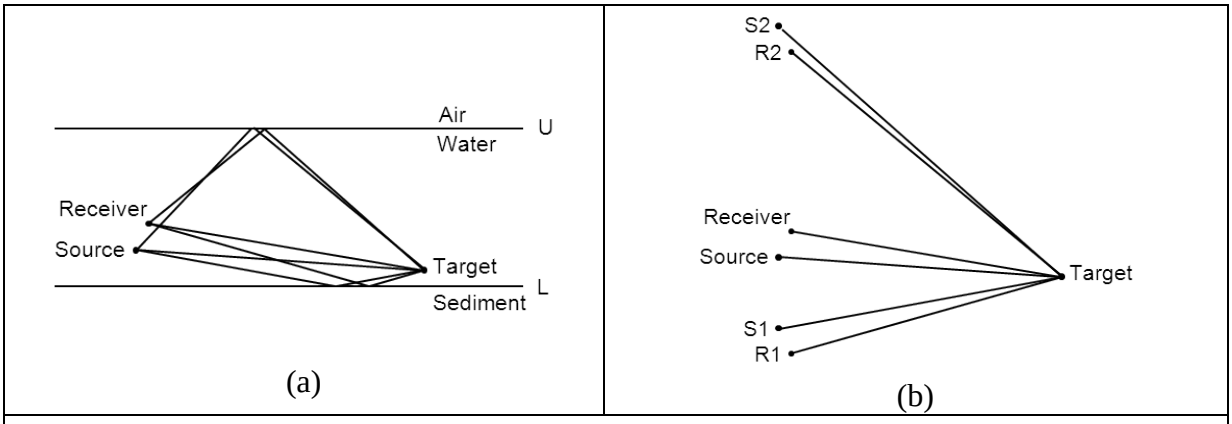

Figure 1: *(a) Acoustic ray diagram showing the direct path arrival and the ray paths associated with a single interaction with the upper and/or lower boundaries of the waveguide. (b) Image sources (S_1, S_2, …) and receivers (R_1, R_2, …) reduce the scattering from a target in a waveguide into a series of free-field scattering problems.*

For an image source, an image receiver, and a target located at $\boldsymbol{r}_i$, $\boldsymbol{r}_j$, and $\boldsymbol{r}_t$, the horizontal distances are $R_{ti} = |\boldsymbol{R}_t - \boldsymbol{R}_i|$ and $R_{jt} = |\boldsymbol{R}_j - \boldsymbol{R}_t|$, and the total separation distances are $d_{ti} = |\boldsymbol{r}_t - \boldsymbol{r}_i|$ and $d_{jt} = |\boldsymbol{r}_j - \boldsymbol{r}_t|$, respectively. In the enumeration of image sources and receivers, $i = 0$ and $j = 0$ correspond to the actual source and receiver. The contribution of the i^{th} source and the j^{th} receiver to the frequency spectrum of the total scattered signal can be written as

$$P_{ij}(\omega) = \left[U^{n(j)} L^{m(j)} \frac{\exp(i\omega t_{jt})}{d_{jt}} \right] \left[U^{n(i)} L^{m(i)} \frac{\exp(i\omega t_{ti})}{d_{ti}} \right] f(\theta_{ij}, \varphi_{ij}, \omega) P_{src}(\omega), \tag{1}$$

where ω is the angular frequency and $P_{src}(\omega)$ is the frequency spectrum of the transmitted wave packet. The reflection coefficients at the upper and lower boundaries are $U(\theta)$ and $L(\theta)$. Here, θ denotes a local grazing angle at the boundary, and is given by $\cos(\theta_i) = R_{ti} / d_{ti}$ or $\cos(\theta_j) = R_{jt} / d_{jt}$. The m and n exponents indicate the number of interactions a ray has with a given interface. The time delay for propagation from the source to the target is $t_{ti} = d_{ti} / c$ and the time delay from the target to the receiver is $t_{jt} = d_{jt} / c$. The speed of sound in the water is c. In (1), the sources and receivers are assumed to be point-like with omni-directional directivity patterns. The scattering process is a convolution of a free-field scattering amplitude $f(\theta_{ij},\phi_{ij},\omega)$ with the incident pressure spectrum $P_{src}(\omega)$. Here, θ_{ij} and ϕ_{ij} are target-centered angles, which are related to the θ_i and/or θ_j and may also depend on the orientation of the target within the waveguide.

The free-field scattered pressure in the far-field of a target is $p_{src} \approx p_0 f(\theta,\phi) \exp(ikr) / r$, where the wavenumber is $k = \omega / c$, $f(\theta,\phi)$ is a scattering amplitude with spherical coordinate polar and azimuthal angles θ and φ [2], and p_0 is a constant carrying the units of pressure. For a finite target, the scattering amplitude is often related to the scattering form function by $f(\theta,\phi) = aF(\theta,\phi) / 2$ with a being a characteristic dimension of the target. Inspection of p_{src} shows that the target is point-like, where the directionality of the scattered field is contained within $f(\theta,\phi)$ along with information about the material properties of the target. Finally, $f(\theta_{ij},\phi_{ij},\omega)$ can be obtained from an analytic solution to a scattering problem (e.g., scattering from a spherical target), direct measurement from an actual target, or numerical simulation (e.g., finite-element analysis).

3. APPLICATION OF THE MODEL TO CIRCULAR SAS

As an example, the waveguide model in (1) is applied to a monostatic circular SAS (CSAS) scenario where the duration of the generated time signals is such that arrivals from the air-water interface are excluded. This then yields four rays paths where $i = 0,1$ and $j = 0,1$. For simplicity, we use $d_0 = d_{t0} = d_{0t}$ and $d_1 = d_{t1} = d_{1t}$. The total frequency spectrum is then given by

$$P(\omega) = \left[f_1 \frac{\exp(i\omega t_1)}{d_0^2} + 2L(\theta_g) f_2 \frac{\exp(i\omega t_2)}{d_0 d_1} + L^2(\theta_g) f_3 \frac{\exp(i\omega t_3)}{d_1^2} \right] P_{src}(\omega), \quad (2)$$

with $t_1 = 2d_0/c$, $t_2 = (d_0 + d_1)/c$, and $t_3 = 2d_1/c$, and the grazing angle is θ_g. The scattering amplitudes, $f_k = f_k(\theta_{ij},\phi_{ij},\omega)$, depend on the locations of the sources, receivers, and target, and target orientation (in the Fraunhoffer region, and equivalent expression with some useful angle definitions can be found in [6]. Eq. 3). An inverse Fouier transform of $P(\omega)$ then gives a generated sonar signal that includes the four primary acoustics paths for a target near an interface. The first term in the bracket of (2) is the direct path. The second term includes the two paths that interact with the bottom once. These paths are reciprocal and are associated with a bistatic scattering direction. The last term is a backscattering path with two bottom interactions.

For the results presented here, the target is placed at the center of the CSAS path. It is a machined aluminum replica of a solid steel artillery shell, which was deployed during Pond Experiment 2010 (PondEx10). In (2), we use a free-field scattering amplitude derived from a hybrid 2D/3D model. The hybrid 2D/3D model implemented a 2D finite-element model (FEM) prediction of the target response on a surface near the target, and then propagates the target response to some specified range using a discrete form of the 3D Helmholtz integral with a free-field Green function [7-9]. The hybrid 2D/3D model can be applied to targets with a cylindrical symmetry. A target drawing and the FEM mesh is depicted in Fig. 2. This scattered pressure is converted to a scattering amplitude

Figure 2: *Engineering rendering of the aluminium replica of a solid steel artillery shell and the FEM mesh. The nodes of the mesh are concentrated near the fine-scale structures of the target. The diameter is 4 inches and the length is 16.*

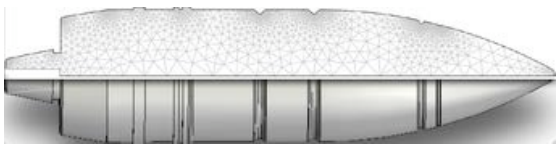

and placed in a table, f_{ijk}, with $\theta_i = i\Delta\theta$, $\phi_j = j\Delta\phi$, and $\omega_k = k\Delta\omega$. Given the source and receiver locations along the circular path and the local grazing for the target location, values of θ and ϕ are determined. Linear interpolation was then employed to extract scattering amplitude values from the table.

Two simulations were performed with the radii of the CSAS path of 5 and 10 m, and adjacent signals were recorded at $\Delta\theta = 1°$ along the circular path. The source and receiver were co-located 3.8 m above the sediment and were assumed to be omni-directional. The sound speed and density of the water are $c = 1500$ m/s and $\rho = 1000$ kg/m^3. The sediment was an attenuating fluid with $c_s = 1775$ m/s, $\rho_s = 2000$ kg/m^3, and $\delta = 0.008$ for the loss parameter. The source emitted a 6 ms chirp with a carrier frequency of 16 kHz and bandwidth of 30 kHz. These parameters roughly correspond to experimental conditions during PondEx10. Figure 3 shows the acoustics color templates obtained from PondEx10 data, FEM simulations, and the ray model.

Acoustic color templates depict the target strength as a function of frequency and a target-centered aspect angle projected onto the water-sediment interface [6].

Inspection of Fig. 3 shows that both the FEM and ray model results capture much of the structure observed in the PondEx10 data. This structure includes both geometrically reflected acoustic energy and acoustic energy that couples into the elastic response of the target. Comparison of Figure 3(b) and (c), particularly in the −10 to −17 dB range, reveals that the ray model result has a slight smoothing. This is a consequence of the discrete representation of f_{ijk} and the linear interpolation. The good agreement may be anticipated because a free-field FEM and Helmholtz integral result for a target at a 10 m range was used in the tabulation of the f_{ijk}.

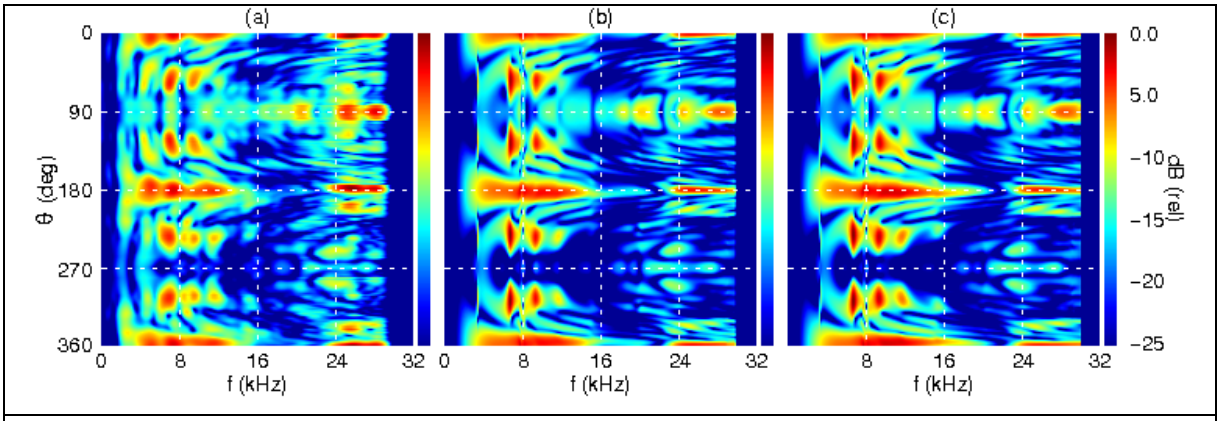

Fig 3: Acoustic color templates for the aluminum replica at a 10 m range. (a) PondEx10 measurement. (b) FEM and Helmholtz integral result. (c) Ray model using the tabulated form function. The tail of the target is pointing at the source/receiver location at 90°; while the nose points at the source/receiver at 270°.

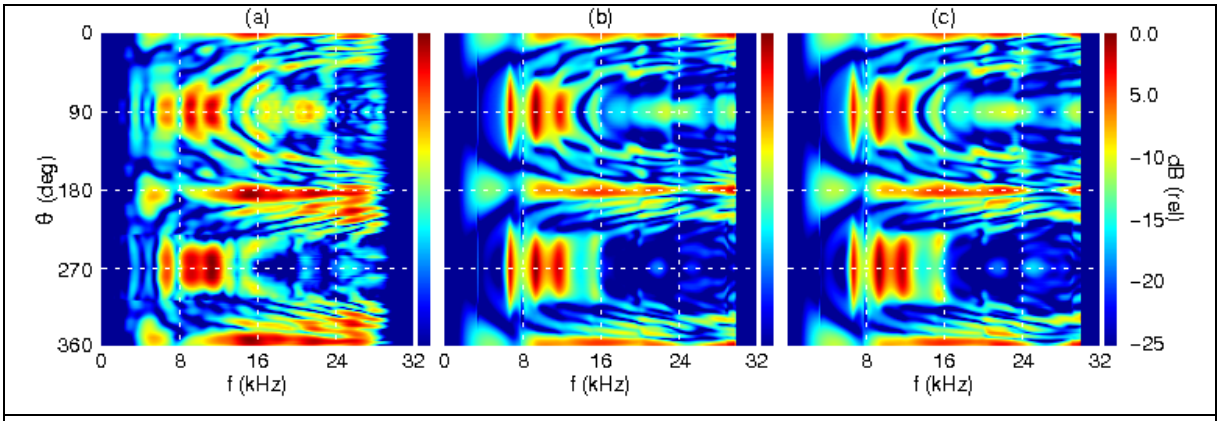

Fig. 4: Acoustic color templates for an aluminum replica at a 5 m range. (a) PondEx10 data. (b) FEM model and Helmholtz integral result. (c) Ray model using the tabulated form function.

Figure 4 shows the PondEx10 data for the aluminum replica, FEM and Kirchoff-Helmholtz integral simulation, and the ray model given in (2) for the target at a 5 m range. An important aspect of the ray model simulation is that it used the table f_{ijk} that was derived from a free-field FEM and Helmholtz integral simulation for a target at a 10 m range. This is possible because the scattering amplitude is range independent and contains only information about the directionality of the scattering and material properties of the target. The construction of the model in Eq. (2)

explicitly accounts for interactions with the water-sediment interface. Thus, only a single free-field measurement from a target or a single free-field FEM and Helmholtz integral simulation is sufficient to provide a scattering amplitude that can be used to rapidly predict the scattering from a target near a bound at any range (provided the range meets the far field requirement).

4. CONCLUSIONS

Section 2 presented a model that combines a ray-based description of wave propagation in a waveguide with a far-field approximation for the free-field scattering from a target. In Sec. 3, the model given in Sec. 2 was applied to a circular SAS example for a proud target where interactions with the upper boundary could be ignored (e.g., due to time gating). Figures 3 and 4 demonstrate that the ray model captures the structure observed in both experimental data and an alternate simulation that used the hybrid 2D/3D model. At the time that Fig. 3(b) and 4(b) were computed, a hybrid 2D/3D model result took 2 to 3 days to complete. The ray model results depicted in Fig. 3(c) and 4(c) took on the order of 30 CPU seconds. Thus, the ray model retains most of the high fidelity of the hybrid 2D/3D model at a fraction of the computational resources.

5. ACKNOWLEDGEMENTS

Work supported by the Strategic Environmental Research and Development Program (SERDP) and the Office of Naval Research (ONR).

REFERENCES

[1] **JE Piper, R Lim, EI Thorsos, KL Williams**, Buried sphere detection using synthetic aperture sonar, *J. Ocean. Eng*., volume 34, pp. 485-494, 2009.

[2] **SG Kargl, KL Williams, EI Thorsos**, Synthetic aperture sonar imaging of simple finite targets, *J. Ocean. Eng*., volume 37, pp. 516-532, 2012.

[3] **JA Bucaro, BH Houston, M Saniga, LR Dragonette, T Yoder, S Dey, L Kraus, L Carin**, Broadband acoustic scattering measurements of underwater unexploded ordnance (UXO), *J. Acoust. Soc. Am*., volume 123, pp. 738-746, 2008.

[4] **J Stack**, Automation for Underwater Mine Recognition: Current Trends & Future Strategy, in *Detection and Sensing of Mines, Explosive Targets, and Obscured Targets XVI*, ed. by RS Harmon, JH Holloway Jr., JT Broach, *Proc. of SPIE*, vol. 8017, 2011 DOI: 10.1117/12.884475.

[5] **KL Williams**, An effective density fluid model for acoustic propagation in sediments derived from Biot theory, *J. Acoust. Soc. Am.*, volume 110, pp. 2276-2281, 2001.

[6] **KL Williams, SG Kargl, EI Thorsos, DS Burnett, JL Lopes, M Zampolli, PL Marston**, Acoustic scattering from an aluminum cylinder in contact with a sand sediment: Measurements, modeling, and interpretation, *J. Acoust. Soc. Am., volume* 127, pp. 3356-3371 (2010).

[7] **M Zampolli, AL Espana, KL Williams, SG Kargl, EI Thorsos, JL Lopes, JL Kennedy, PL Marston**, Low- to mid-frequency scattering from elastic objects on a sand sea floor: simulation of frequency and aspect dependent structural echoes, *J. Comput. Acoust*., volume 20, pp. 1240007 (14 pp.), 2012.

[8] **M Zampolli, A Tesei, G Canepa, OA Godin**, Computing the far field scattered or radiated by objects inside layered fluid media using approximate Green's functions, *J. Acoust. Soc. Am.*, volume 123, pp. 4051-4058, 2008.

[9] **M Zampolli, A Tesei, FB Jensen, N Malm, JB Blottman III**, A computationally efficient finite element model with perfectly matched layers applied to scattering from axially symmetric objects, *J. Acoust. Soc. Am.*, volume 122, pp. 1472-1485, 2007.

Enclosure 3

Fast Ray Model Deficiency:

A fast ray model developed in FY11 assumed a homogeneous layer of water. Rays are assumed to travel in straight line segments from a source to a receiver. For an interaction of a ray with an interface, an appropriate reflection coefficient is included in the received signal. For an image located at $\boldsymbol{r}_i$ and a receiver located at $\boldsymbol{r}_r$, the horizontal and total separation distances are $|\boldsymbol{R}_r - \boldsymbol{R}_i|$ and $|\boldsymbol{r}_r - \boldsymbol{r}_i|$, respectively. The contribution of the ith image to the frequency spectrum at the receiver can be written as

$$P_i(\omega) = P_{src}(\omega) s_0 \left[A^n(\theta_i) B^m(\theta_i) \frac{\exp(i\omega t_i)}{|\vec{r}_r - \vec{r}_i|} \right], \tag{1}$$

where $P_{src}(\omega)$ is the frequency spectrum of the transmitted wave packet and s_0 is a reference distance used in the calibration of the source level. The reflection coefficients at the upper and lower boundaries are $A(\theta_i)$ and $B(\theta_i)$, where the local grazing angle θ_i at a boundary is given by $\cos(\theta_i) = |\boldsymbol{R}_r - \boldsymbol{R}_i| \,/\, |\boldsymbol{r}_r - \boldsymbol{r}_i|$, and the m and n exponents indicate the number of interactions a ray has with a boundary. The time delay for propagation is $t_i = |\boldsymbol{r}_r - \boldsymbol{r}_i|/c$ with c being the speed of sound in the water.

During FY13, simulations of scattering from a 15-m radius fluid sphere in a 4000-m deep Pekeris waveguide with source-receiver-target separation distances on the order of 100 km revealed the implementation of the propagation component of the fast ray model violated reciprocity under certain conditions. If the source and receiver were located below the mid-depth of the Pekeris waveguide, the implementation satisfied reciprocity. If, however, either the source or receiver or both were above the mid-depth of the waveguide, then reciprocity failed.

The failure was caused by a change in the enumeration of image sources, the method used to determine the reflection coefficient exponents, and the selection of images that contribute within a time window of interest. The depth of the waveguide is h, and the actual source is located at z_s (> 0) with the seafloor at $z = 0$. The first image was below the seafloor at $z_1 = -z_s$. Additional images were added in quartets, because images planes were added in pairs, symmetrically about the seafloor. The qth quartet of image was added to the set of image with the following z-coordinates: $2qh + z_s$, $2qh - z_s$, $-2qh - z_s$, and $-2qh + z_s$ with $q = 1, 2, 3, \ldots$. The ordering assumed that $z_s < h/2$, and the determination of the reflection coefficients assumed that the ray associated with the first image always interacted with the seafloor and the rays in the enumeration of the remaining image source then alternated with interacting with the air-water interface and seafloor. As long as $z_s < h/2$, $z_1 = -z_s$, and the addition of quartets followed the prescribed ordering, then the images were sorted in a manner consistent with the determination of the m and n exponents in Eq. (1), and reciprocity was ensured.

In the FY13 simulations with separation distances on the order of 100 km, it was advantageous to consider only a finite length time window, t_w, with a defined time offset, t_o. It then followed that only images with propagation delays $t_i = |\boldsymbol{r}_r - \boldsymbol{r}_i|/c$ within the time window needed to be considered; and so, the set of image were sorted such that $t_o \le t_i \le t_w$ and $t_i < t_{i+1}$ When $z_s > h/2$, the new sorting led to a first image with $z_1 = 2h - z_s$, and the ray associated with it reflects initially from the air-water interface. The implementation of the new model failed to updated the determination of m and n, and thus, reciprocity was violated.

The set of images, which contribute to the pressure spectrum, are selected from the set constructed in the following manner. First, for a source located at $r_s = (x_s,y_s,z_s)$ and $0 < z_s < h$, coordinates for all images have $x_i = x_s$ and $y_i = y_s$. The coordinates for N images (including the actual source) are first constructed in an unsorted manner:

$$\begin{aligned} z_1 &= z_s, \quad \text{(actual source)} \\ z_2 &= -z_s, \\ z_{q+3} &= 2qh + z_s, \\ z_{q+4} &= 2qh - z_s, \\ z_{q+5} &= -(2qh - z_s), \\ z_{q+6} &= -(2qh + z_s), \end{aligned} \tag{3}$$

where $q = 0, 4, 8, \ldots$ and $q + 6 < N$. Next, the images are sorted by the $d_i = |z_i - z_1|$ with $i = 2, 3, ..., N$ and $d_i < d_{i+1}$. This then guarantees the ordering of delay times: $t_i < t_{i+1}$.

The detemination of the reflection coefficient exponents then follows from the symmetry imposed by the seafloor at $z = 0$ and whether $z_2 < z_s$ or $z_2 > z_s$. If the former, the ray tracing of the first few rays yields the sequences of reflection coefficients:

$$\begin{aligned} &i = 1, && \text{(actual source)} \\ &i = 2, && B, & \qquad &i = 3, && A, \\ &i = 4, && AB, & \qquad &i = 5, && BA, \\ &i = 6, && BAB, & \qquad &i = 7, && ABA, \\ &i = 8, && ABAB, & \qquad &i = 9, && BABA, \\ &i = 10, && BABAB, & \qquad &i = 11, && ABABA, \end{aligned} \tag{4}$$

For the latter situation, the ray tracing gives

$$\begin{aligned} &i = 1, && \text{(actual source)} \\ &i = 3, && B, & \qquad &i = 2, && A, \\ &i = 5, && AB, & \qquad &i = 4, && BA, \\ &i = 7, && BAB, & \qquad &i = 6, && ABA, \\ &i = 9, && ABAB, & \qquad &i = 8, && BABA, \\ &i = 11, && BABAB, & \qquad &i = 10, && ABABA, \end{aligned} \tag{5}$$

The violation of reciprocity in the benchmarks was caused by an unconditional use of (4) where the location of the actual source within the waveguide was ignored.

REPORT DOCUMENTATION PAGE

Form Approved
OMB No. 0704-0188

PLEASE DO NOT RETURN YOUR FORM TO THE ABOVE ADDRESS.

1. REPORT DATE *(DD-MM-YYYY)*	2. REPORT TYPE	3. DATES COVERED *(From - To)*
08-10-2013	Final Technical Report	01-Jan-2010 -- 30-Jun-2013

4. TITLE AND SUBTITLE

Generation of Synthetic SAS Data for Targets Near the Seafloor: Propagation Component

5a. CONTRACT NUMBER

5b. GRANT NUMBER

N00014-110-1-0114

5c. PROGRAM ELEMENT NUMBER

6. AUTHOR(S)

Steven G Kargl, University of Washington

5d. PROJECT NUMBER

5e. TASK NUMBER

5f. WORK UNIT NUMBER

7. PERFORMING ORGANIZATION NAME(S) AND ADDRESS(ES)

Applied Physics Laboratory
University of Washington
1014 NE 40th St.
Seattle, WA 98105

8. PERFORMING ORGANIZATION REPORT NUMBER

9. SPONSORING/MONITORING AGENCY NAME(S) AND ADDRESS(ES)

Office of Naval Research
875 North Randolph Street
Arlington, VA 22203

10. SPONSOR/MONITOR'S ACRONYM(S)

ONR

11. SPONSOR/MONITOR'S REPORT NUMBER(S)

12. DISTRIBUTION/AVAILABILITY STATEMENT

Distribution Statement A: Approved for public release, distribution unlimited.

13. SUPPLEMENTARY NOTES

14. ABSTRACT

Monostatic synthetic aperture sonar (SAS) data sets for the scattering from a target in a waveguide can be simulated via a fast model that combines an acoustic ray approximation for propagation in the waveguide with far-field scattering from a target in free-space. With the assumption that acoustic rays arise from the source and receiver and their images, the problem of wave propagation and scattering from a target within the waveguide is replaced by a superposition of a set of free-field scattering problems. Under normal operating conditions, the separation distance between a SAS platform and a target is large compared to the carrier wavelength of the transmitted signal, and hence, the free-field scattered signal can be reduced to a far-field approximation where a spherically diverging wave is weighted by a scattering amplitude. The scattering amplitude contains all of the information about the scatterer (e.g., its material properties) and the directionality of the scattered field. A scattering amplitude can be obtained from a direct measurement or a finite-element analysis of a target. The fast ray model allows one, who is interested in SAS processing algorithms, to generate data sets with variations in the environment or source-receiver-target geometry without incurring the

15. SUBJECT TERMS

Acoustic Ray Model, Synthetic Aperture Sonar, Scattering amplitude

16. SECURITY CLASSIFICATION OF:			17. LIMITATION OF ABSTRACT	18. NUMBER OF PAGES	19a. NAME OF RESPONSIBLE PERSON
a. REPORT	b. ABSTRACT	c. THIS PAGE			Steven G Kargl
U	U	U	U	11	19b. TELEPHONE NUMBER *(Include area code)* (206) 685-4677

Reset

Standard Form 298 (Rev. 8/98)
Prescribed by ANSI Std. Z39.18